CrossMark

Space Weather at Comet 67P/Churyumov–Gerasimenko Before its Perihelion

S. McKenna-Lawlor[1] · W. Ip[2] · B. Jackson[3] · D. Odstrcil[4] ·
P. Nieminen[5] · H. Evans[5] · J. Burch[6] · K. Mandt[6] ·
R. Goldstein[6] · I. Richter[7] · M. Dryer[8]

Abstract Interplanetary scintillation observations, as well as the ENLIL 3D-MHD model when employed either separately or in combination with the observations, enable the making of predictions of the solar wind density and speed at locations in the inner heliosphere. Both methods are utilized here to predict the arrival at the Rosetta spacecraft and its adjacent comet 67P/Churyumov–Gerasimenko of, flare related, interplanetary propagating shocks and coronal mass ejections in September 2014. The predictions of density and speed variations at the comet are successfully matched with signatures recorded by the magnetometer and the ion and electron sensor instruments in the Rosetta Plasma Package, thereby providing confidence that the signatures recorded aboard the spacecraft were solar related. The plasma perturbations which were detected some 9–10 days after significant flaring in September 2014 are interpreted to have been signatures of the arrivals of three coronal mass ejection related shocks at the comet. Also, a solar energetic particle event was recorded at 3.7 AU within $\sim$30 min of the onset of a flare by the Standard Radiation Monitor aboard Rosetta.

✉ S. McKenna-Lawlor
stil@nuim.ie

[1] Space Technology Ireland, Ltd., NUI Maynooth, County Kildare, Ireland

[2] National Central University, 300 Chung-Da Rd., Chung-Li 32054, Taiwan

[3] University of California San Diego, 9500 Gilman Drive, La Jolla, CA, USA

[4] Goddard Space Flight Centre, 8800 Greenbelt Rd., Greenbelt, MD 20771, USA

[5] ESA's European Space Research and Technology Centre, Noordwijk, The Netherlands

[6] Southwest Research Institute, 6220 Culebra Rd., San Antonio, TX, USA

[7] Technische Universität Braunschweig, Mendelssohnstrasse 3, 38116 Brunswick, Germany

[8] NOAA Space Weather Prediction Centre (RET.), Boulder, CO 80305, USA

1 Introduction

Ground based observations of comets, and even close fly-bys of these objects, only provide information concerning species in cometary comae which have already been altered by physiochemical processes (such as sublimation and interactions with solar radiation and the solar wind). The presently ongoing *Rosetta Mission* (Glassmeier et al. 2007a), which is a *Planetary Cornerstone Mission* in the long term program *Horizon 2000* of the *European Space Agency* (ESA), uniquely employs two investigative strategies to overcome this limitation. First, its Lander Philae has the capability to provide 'ground truth' concerning the composition of target comet *67P/Churyumov–Gerasimenko* (67P/C–G) through making an in situ analysis of the material of the nucleus using a suite of 10 on-board instruments. Second, monitoring of the evolving cometary environment is implemented along the trajectory of the spacecraft around the Sun from the time of the emergence of Rosetta from hibernation at about 4 AU on 20 January 2014, through its subsequent injection into an orbit about the comet on 6 August, 2014 at ~ 3 AU. This monitoring, which utilizes the measurements of 10 on-board instruments, is scheduled to continue through the perihelion passage of the comet (at 1.24 AU on 13 August 2015) and will subsequently be sustained post perihelion to an outbound distance of about 2 AU. The mission will terminate at the end of September 2016 when it is planned that Philae will be landed on the surface of the comet.

1.1 Space Weather at the Comet

A *Standard Energetic Particle Radiation Environment Monitor* (*SREM*), Mohammadzadeh et al. (2003) and a suite of plasma instruments (Carr et al. 2007) are flown aboard the Rosetta spacecraft to perform ongoing measurements (during the escort phase of the mission) that monitor the changing interactions between the solar wind and the comet. These interactions are sensitive to changes in the solar wind dynamic pressure, not only as the comet changes its heliocentric distance and activity, but also as the solar wind itself varies in response to transient events on the Sun (the generation of flares and the production of coronal mass ejections (CMEs), e.g. Dryer 1976).

1.2 Present Study Objective and Paper Layout

In the present paper we investigate the response of weakly outgassing comet 67P/C–G to the arrival of a solar energetic particle (SEP) event (Cane et al. 1986; Reames 1999, 2013) and to variations produced by dynamic enhancements in the solar wind associated with the propagation to Rosetta of flare related shocks (ICMEs) (Burlaga et al. 1981; Gopalswamy et al. 2000).

In Sect. 2, a short description of the *Standard Radiation Environment Monitor* (SREM) aboard Rosetta, data from which are used to investigate responses at the comet to SEP arrivals is presented. Instruments in the *Plasma Package* (*RPC*) aboard Rosetta, data from which are in addition used to investigate responses at the comet to solar wind enhancements, are also briefly described.

In Sect. 3 the interplanetary scintillation (IPS) technique time-dependent three-dimensional (3D) reconstruction program used in this study to predict the arrival at Rosetta of flare related disturbances, is outlined. This technique is designed to predict the solar wind speed and density at locations in the inner heliosphere (e.g. Jackson et al. 1998; Jackson and Hick 2005; Jackson 2011). A short account of the ENLIL 3D-MHD model, developed

(Odstrčil 2003) to provide predictions of the arrival of solar disturbances at locations throughout the heliosphere is also described in this section. Both modelling efforts appear on the Web for providing Earth forecasts.

Thereafter, in Sect. 4 accounts of two significant solar flares that occurred in September 2014 are presented. The relationship between solar flaring and one temporally related SEP recorded by the SREM aboard Rosetta is discussed in Sect. 5.

Predictions made using the IPS and ENLIL models of the arrival at Rosetta and its adjacent comet of plasma disturbances associated with the two solar flares described in Sect. 4 are provided in Sect. 6. These predicted arrival times are compared in Sect. 7 with signatures present at the predicted times in MAG and IES data. A discussion is mounted in Sect. 8 of the solar related signatures recorded at the comet and an account presented of the circumstances under which the arrival of dynamic solar events can result in the generation of sputtering from a cometary surface. General conclusions are contained in Sect. 9.

2 Radiation and Plasma Measurements On-Board Rosetta

2.1 Standard Radiation Environment Monitor

A SREM developed by ESA (already mentioned above in Sect. 1.1) one unit of which is currently flown (among several other spacecraft carriers) aboard Rosetta, consists of three silicon detectors (D1, D2 and D3) mounted in a double detector head. One element comprises a single silicon diode detector (D3) and the other utilizes two silicon diodes (detectors D1/D2) in a telescope configuration. SREM detects high energy protons (from ~ 10 to ~ 300 MeV) and electrons (from ~ 300 keV to ~ 6 MeV) in several energy channels and provides energy spectral information with a $\pm 20°$ angular resolution. Correlative studies of events recorded by similar units flown aboard different spacecraft are described in Mavromichalaki et al. (2009).

2.2 The Plasma Package Aboard Rosetta

The plasma package flown by the *Rosetta Plasma Consortium* (RPC) is made up of five sensors (Carr et al. 2007) namely: the *ion and electron sensor* (IES); the *fluxgate magnetometer* (MAG), the *ion composition analyzer* (ICA); the *mutual impedance probe* (MIP) and the *Langmuir probe* (LAP) In the present study, only data recorded at the spacecraft by IES and MAG are used to determine if variations in the measurements recorded at the comet can be contemporaneously matched with the predicted arrivals at Rosetta of solar disturbances. The IES consists of two electrostatic plasma analysers, one each for ions and electrons, which share a common entrance aperture. The instrument provides three dimensional plasma distribution functions of electrons and ions over an energy/charge range that extends, with 4 % resolution, from 1 eV/e to 22 keV/e. Through the use of electrostatic angle scanning, the instrument achieves a field of view of $90° \times 360°$. The angular resolution for electrons is $5° \times 22.5°$ while the angular resolution for ions is $5° \times 45°$—with one $45°$ sector configured to measure the solar wind at a resolution of $5°$ (Burch et al. 2007).

The *fluxgate magnetometer experiment* (MAG) aboard Rosetta is designed to measure the magnetic field present in the interaction region between the solar wind plasma and comet 67P/C–G. The instrument is composed of two tri-axial fluxgate magnetometer

sensors, mounted on a 1.5 m long spacecraft boom. The measurement range of each sensor is ± 16,384 nT, with quantization steps of 31 pT, and the system is operated with a time resolution down to 0.05 s, corresponding to a bandwidth of 0–10 Hz. This performance supports a detailed analysis of magnetic field variations in the environment of the comet (Glassmeier et al. 2007b).

3 Solar Wind Modelling Prediction Techniques

The *interplanetary scintillation 3D-reconstruction technique* (IPS analyses) developed in time-dependent form by the University of California, San Diego, provides precise tomographic 3D-reconstructions of the time-varying global heliosphere. The technique operates by iteratively fitting IPS observations to a kinematic solar wind model that conserves mass and mass flux. These analyses of transient solar wind features can match, and also provide an extended low-resolution global view of, the solar wind parameters speed, density, and vector magnetic fields extrapolated from the solar surface which are usually only measured by in situ sensors (e.g. Jackson 2011). Used with STELab, Japan IPS observations (http://stesun5.stelab.nagoya-u.ac.jp/index-e.html), this technique has been in operation since the year 2000 to predict conditions in real time in the inner heliosphere (see: http://ips.ucsd.edu). Solar data recorded during recent missions (e.g. STEREO, SMEI), have significantly improved the possibility to remotely measure detailed aspects of specific solar transient events near the Sun, including their outflow and three dimensional structure (Jackson et al. 2004, 2006; Kaiser et al. 2008). Such observations show increased solar wind detail that certifies, and can be compared with the results of IPS analyses. Pertinent to this study, a real-time prediction of conditions at comet 67P/C–G updated every 6 h is available at: ftp://cass185.ucsd.edu/data/IPS_Rosetta_Real_Time.

ENLIL is a time-dependent 3D-MHD model of the heliosphere which solves equations for: plasma mass; momentum and energy density; and magnetic field; using a flux-corrected-transport (FCT) algorithm. Its inner radial boundary is typically located at 21.5 solar radii and it can accept boundary condition information from the Wang–Sheely–Arge (WSA) model (Arge and Pizzo 2000). Its outer radial boundary can be adjusted to include planets or spacecraft of interest (in the present case, Rosetta). It covers 60° north to 60° south in latitude and 360° in azimuth (Odstrčil and Pizzo 1999a, b). Both ENLIL and the kinematic 3D-reconstruction analysis can provide extractions at a point location over time from the volumetric data set anywhere within the volume.

The IPS 3D-reconstruction results can also be extracted at any solar distance as two-dimensional maps over time within the reconstructed volume and exploited to provide inner boundary values to drive the ENLIL three-dimensional (3D)-MHD model from archival data (Yu et al. 2015) or in near real time (Jackson et al. 2015). Some of the heliospheric analyses presented below utilized ENLIL 3D-MHD modelling from IPS-derived 3D reconstructions, and versions of these and other models using ENLIL are presented at George Mason University, VA in: http://spaceweather.gmu.edu/projects/enlil/.

4 Significant Solar Activity in September 2014

Solar Cycle 24 has, thus far, been characterized by presenting a relatively low level of solar activity. Never-the-less, a significant number of solar energetic events has been recorded since the Rosetta instruments resumed operations on 20 January, 2014, following a long

hibernation. In this paper two of these events are discussed. Event 1 (September 1, 2014) and Event 2 (September 10, 2014). Figure 1 (left) shows the relative positions of the Sun, Earth the STEREO spacecraft and the comet on 11 September 2014 at 09:00 UT in an ecliptic projection. This figure shows a density enhancement to the East of Rosetta (clockwise) associated with, and following, a CME on 1 September (see below) that had reached well beyond Rosetta's distance from the Sun at this time. Figure 1 (right) provides a contemporaneous meridional cut. An ENLIL 3D-MHD model analysis for the same time is presented in Sect. 6.

4.1 The Solar Event of 1 September 2014

A flare which originated on the far side of the Sun took place on 1 September in Active Region 12158 when it was located just beyond the north-eastern limb. It was, thus, not visible from Earth but a major particle event at E126° (N. Nitta, private communication) was recorded at about 11.00 UT on 1 September 2014 aboard NASA's Solar TErrestrial RElations Observatory (STEREO) which was behind the Sun. Further, NOAA/USA/ Australia's Ionospheric Service reported that metric Type II radio observations made at Culgoora had yielded a speed for an accompanying coronal shock of $V_s = 2019$ km/s. The plane of sky (POS) speed of the related CME when recorded aboard the *Solar Heliospheric Observatory* (*SOHO*) spacecraft LASCO C2 and C3 coronagraphs (Howard et al. 2008) at L1, was (as averaged by the outward motion in C2 and C3) $V_{cme} \sim 2216$ km/s (K. Schenk, private communication). A dimming event was observed from Earth at the west limb which was propagated by this solar activity.

Figure 2 presents various data from the GOES-15 spacecraft recorded from 01 September 00:00 UT to 30 September 24 h UT. These plots show that on 1 September electrons arrived at Earth close to the time of initiation of the parent flare. For information on the protons see Sect. 5.
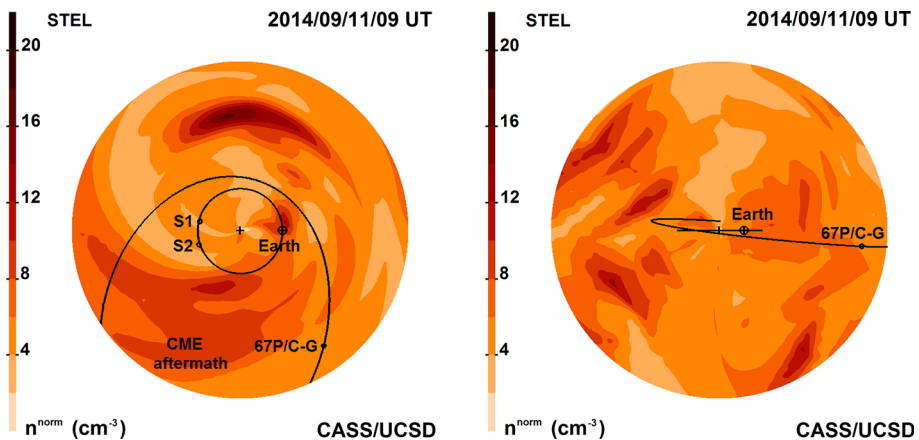

Fig. 1 *Left* An ecliptic cut showing the relative positions of the Sun, Earth, the STEREO spacecraft and comet 67P/C–G on 11 September 2014 at 09.00 UT, *right* a contemporaneous meridional cut including comet 67P/C–G. Earth's orbit is projected as a *straight horizontal line* in this figure. Both cuts are shown against a background solar wind density model derived using IPS 3D kinematic reconstructions normalized to values at 1 AU
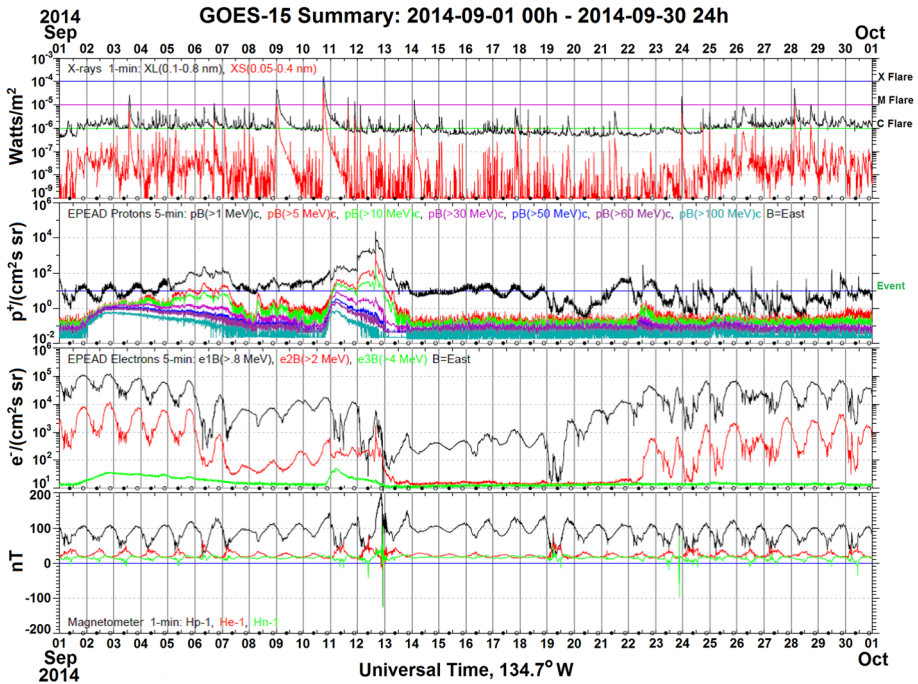
Fig. 2 Various GOES 15 data recorded from 01 September 00 h to 30 September 24 h, *panel 1* (*top*), X-rays: XL (0.1–0.8 nm) and XS (0.05–0.4 nm); *panel 2*, EPEAD protons: energies >1, >5, >10, >30, >50, >60, >100 MeV; *panel 3*, EPEAD electrons, energies >8, >2, >4 MeV; *panel 4* magnetic data in nT

4.2 The Solar Events of 9–10 September

A long duration M4.5 solar flare (also in active region AR 12158), which reached a peak at 00:29 UT on 9 September 2014, was associated with the generation of Type II and Type IV radio emissions. A CME became visible shortly thereafter in LASCO C2 imagery and, based on these data, although most of the ejected plasma appeared to be headed north-eastward, a weaker Earth directed component was seen which was predicted to arrive at Earth either late on 11 September or early on 12 September 2014 (see below).

A further solar flare (measuring X1.6 at its peak time) erupted at 17:32 UT on 10 September 2014, again in complex active region AR 12158 which, on that day, was located almost at the centre (N15, E09) of the solar disk (event peak: 17:45 UT; event end: 18:20 UT). Also, a CME accompanied by a metric Type II burst with an estimated shock speed of $V_s = 3750$ km/s was recorded as well as accompanying Type IV radio emissions. The POS speed of this (halo) CME event (which was observed by LASCO aboard SOHO to be headed directly towards Earth) was $V_{cme} = 1416$ km/s. The SOHO C2 white light image showed the propagating shock to have a speed of $V_s = 1800$ km/s (K. Schenk, private communication).

The first CME arrived at Earth on 11 September at 23:47 UT where it produced a sudden commencement (SC) registered by low-latitude magnetometers operated by the Geomagnetism Program of the US Geological Survey. See the first SC as recorded at the San Juan magnetic observatory (Fig. 3, bottom panel). The arrival of this structure was
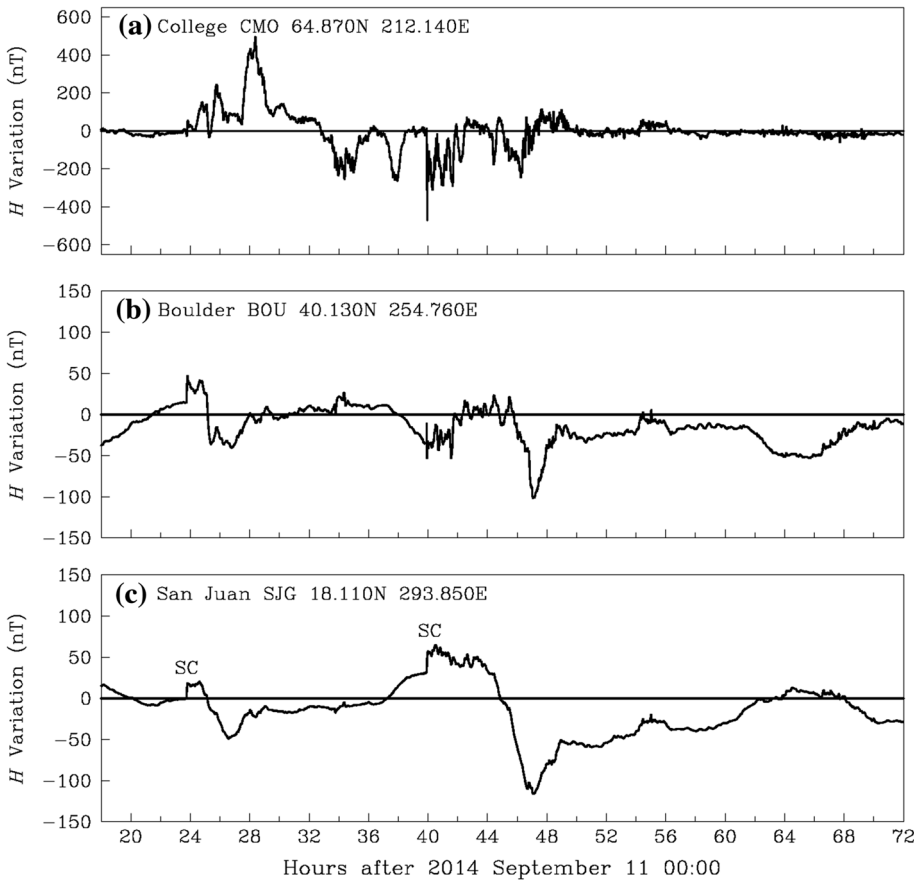
Fig. 3 Signatures of magnetic storms at Earth associated with the arrival of CMEs associated with flaring on 9 and 10 September 2014. For details see the text

marked by an increase in the solar wind velocity from 400 to about 480 km/s. The second CME arrived on 12 September at 15:57 UT and, this time, the solar wind velocity jumped from 450 to about 620 km/s. Over the next 24 h the main-phase of a magnetic storm (associated with a west-ward-directed, equatorial magnetospheric electric current) was activated which lead to a characteristic depression in the low-latitude magnetic distur-bance, NOAA reported a $Kp = 7$ magnetic index, which is indicative of a "strong" magnetic storm. It is noteworthy that at high-latitudes (Fig. 3, top panel), the magnetic disturbance was typical of a magnetic storm with a much greater amplitude.

5 SREM Data

Between 30 August and >9 September 2014, three energy channels of SREM/Rosetta, which are sensitive to protons with energies >12, >27 and >49 MeV respectively, recorded a significant particle enhancement (Fig. 4). A good correlation between energetic particle data recorded by the SREM unit aboard Rosetta and the counts measured by an
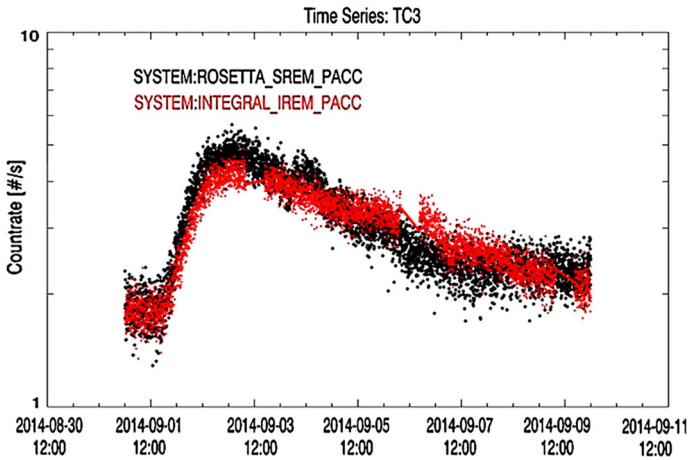
Fig. 4 SREM data recorded aboard the Rosetta spacecraft (*black font*) and the Integral spacecraft (*red font*) from 12:00 UT on 30 September to 12:00 UT on 11 September 2014 in complementary channels sensitive to protons with energies E > 27 MeV
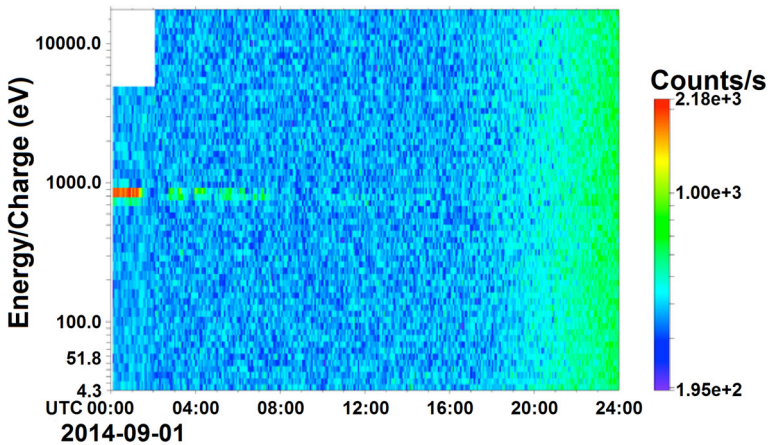

Fig. 5 Counts summed over elevations and azimuth in the IES instrument on 1 September 2014

identical SREM aboard the Earth-orbiting INTEGRAL spacecraft (Pace et al. 1994) was found—see Fig. 4 which compares the count rates contemporaneously measured aboard SREM/Rosetta and SREM/Integral at E 27 MeV. It should be noted that protons arrived at Rosetta approximately half an hour before they reached Earth while also the flux levels were higher at Rosetta than at Earth.

It is noted that the spikes seen in the integral plot result from periodic passages of the spacecraft through the Earth's radiation belts.

Figure 5 shows, relative to counts summed over elevations and azimuth in the IES on 1 September 2014, a rising background of solar protons due to the waxing SEP event. These protons caused the instrument to saturate towards the end of 1 September and also on the following day.

Fig. 6 SREM/Rosetta flux measurements in various energy channels between 25 August and 30 September 2014 (Sandberg et al. 2012)

No enhancement in SREM data was recorded (Fig. 6) in association with the SEP recorded at Earth on 10–11 September 2014 (compare with Fig. 2).

6 Predictions of the IPS and ENLIL Models of Shock/CME Arrivals at Rosetta in Association with Events 1 and 2

Following the time when IPS data are measured in association with a particular solar event, reconstructive analysis is carried out to allow material propagating outward from near the Sun to be followed to the edge of the analysis volume (in the case of Rosetta this edge is at 4 AU). The propagation outward of density/speed following the time the initial data are recorded defines a "prediction". For the WSA-driven ENLIL, the time from which data are measured (during the event) is from their passage at the solar surface to the lower corona. For the IPS 3D-reconstructions or the IPS-driven ENLIL model, data are recorded from the time of their passage from the inner heliosphere out to about 2.0 AU.

ENLIL modelling helped to illuminate the aftermath of the very large and high speed CME on 1 September, 2014 that was described in Sect. 4.1. Using a WSA solar wind background and cone model inputs to ENLIL (see Taktakishvili et al. 2009), the modelling produced a fast pulse of energy, and a shock at the Sun that can be seen in the modelling accumulating intervening material and almost reaching to the distance of Rosetta on 11 September 2014 (Fig. 7).

The dense structure along the Sun–Earth line beyond 2 AU is most likely from another more Earth-directed CME. In this case, the IPS STELab, Japan observations missed most of the very fast CME (see Fig. 1) that began slightly after the array stopped operating in the evening, local time; by the next day the front of this large event had mostly passed beyond the field of view of the STELab IPS system.

Figure 8 (left) presents the IPS-3D reconstructed heliospheric density (red font) values at Earth determined from a kinematic tomographic analysis made using STELab, Japan IPS
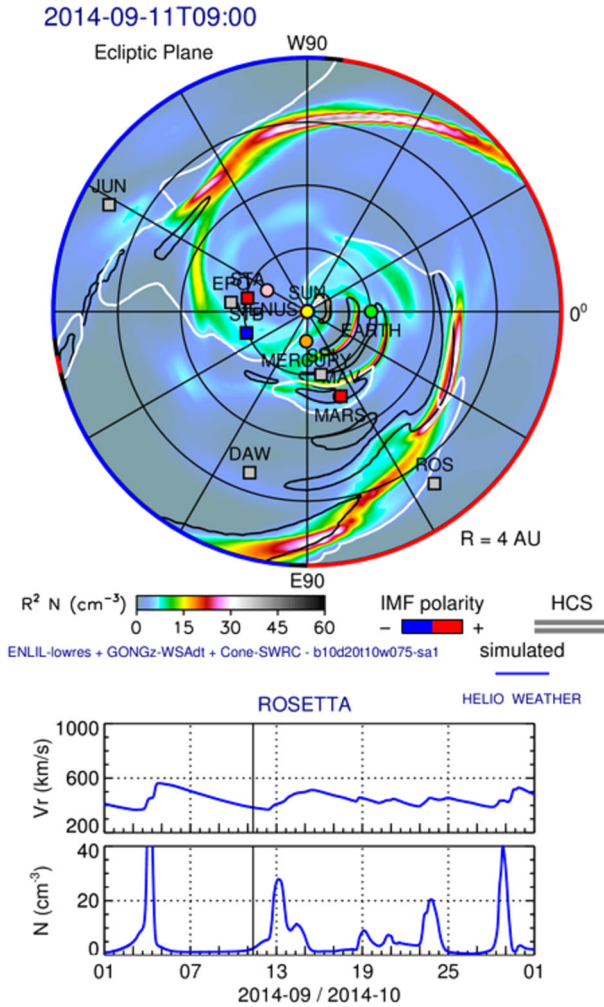
Fig. 7 *Top* A WSA-cone model driven ENLIL model is shown in a heliographic equatorial plot indicating the aftermath location of the enhancement in density as an accumulation of swept-up material and a shock front, determined at 9:00 UT on 11 September 2014. The values of density have been normalized to those at 1 AU. The projected locations of many inner heliospheric spacecraft and planets are labeled, including Earth and Rosetta. The heliospheric current sheet/HCS sector boundaries in interplanetary space projected onto the ecliptic are shown by a *white line* (represented in the icon between parallel *bars*). *Bottom* Heliospheric speed and density values from WSA-cone ENLIL modelling at Rosetta. The *vertical solid timeline* shows the approximate time of the event observed at Rosetta

data over the interval from 3 September to 2 October. These tomographic values are compared with in situ measurements (black line) obtained at the *Wind* spacecraft (Ogilvie and Parks 1996). It is noted that the level of the signal at Earth was suitably matched with the tomographic values determined from IPS tomography. The coefficient of correlation between measured in situ values and predicted data is 0.928 (Fig. 8, right).

The large peak in density at Earth on 12 September includes a significant amount of material, partly from the CME associated with the M4.5 flare on 9 September followed, 16 h later, by
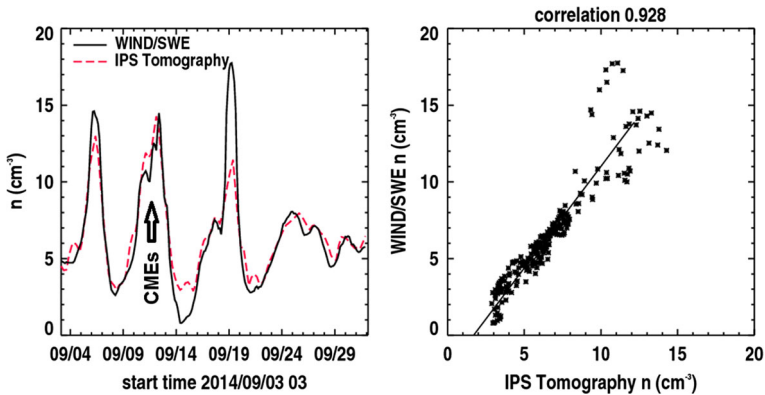
Fig. 8 *Left* Heliospheric density values (*dashed red line*) at Earth determined from a tomographic analysis made using STELab. Japan IPS data recorded over a month in September 2014, shown compared with in situ measurements obtained at the Wind spacecraft. The Wind data have been averaged with a one-day boxcar to approximate the resolution of the IPS 3D–reconstruction. The locations of the CMEs initiated on 9–10 September are indicated by the *arrow*. *Right* Correlation between measured and predicted data

material associated with the X1.6 flare and halo CME on 10 September that arrived with a large shock at 15:57 UT on 12 September (as described in Sect. 4.1). Figure 9a (top left) shows complementary heliospheric speed values at Earth obtained using the same kinematic tomographic analysis adopted in Fig. 8 based on STELab. Japan IPS data compared with in situ measurements obtained at the Wind spacecraft. The correlation coefficient between measured and predicted data (Fig. 9a top right) is 0.858. The bottom plots (Fig. 9b) present heliospheric speed and density values from IPS driven ENLIL modelling at Earth compared with OMNI, hour-averaged, in situ measurements made over approximately the same time interval.

Figure 10 shows (left) the density and (right) the speed at Rosetta derived from IPS tomography using the same analysis procedure adopted for Figs. 8 and 9. Note the large density increase at around 18–20 September 2014. This density enhancement was composed of material from at least the two closely spaced CMEs tracked outward from the times of their respective launches on 9 and 10 September 2014 in ecliptic and meridional cuts. The material interacted *en-route* with a co-rotating structure. The density increase at Rosetta was associated with several shocks observed at Earth whose location is not well-depicted in the IPS kinematic modelling as they propagated further into the heliosphere.

To track the shocked response it is better to use ENLIL 3D-MHD modelling, as in Fig. 11. Here, in the IPS driven ENLIL modelling, the density increase shown in the IPS kinematic analysis peaks up more at the time of the peak density at Rosetta on 18–20 September. The derived speeds from both the kinematic and 3D-MHD modeling were within 100 km/s of being constant throughout this period in the Rosetta 3D-reconstructions. The speed (Fig. 10 right) was observed to peak in the IPS kinematic modelling on 11 September and this is very likely an outflow aftermath associated with the large CME initiated on 1 September that is shown in WSA ENLIL modelling as a density enhancement at about the same location at the later time. A sustained speed from the Sun of about 600 km/s would have needed to be present nearly 90° from the associated CME propagation direction to produce this enhancement at Rosetta. Both of the solar disturbances present at Rosetta (on 11 September) and the density increase on 19 September agree with the timings of two enhanced solar wind ion measurements recorded at Rosetta in the IES instruments (next section).
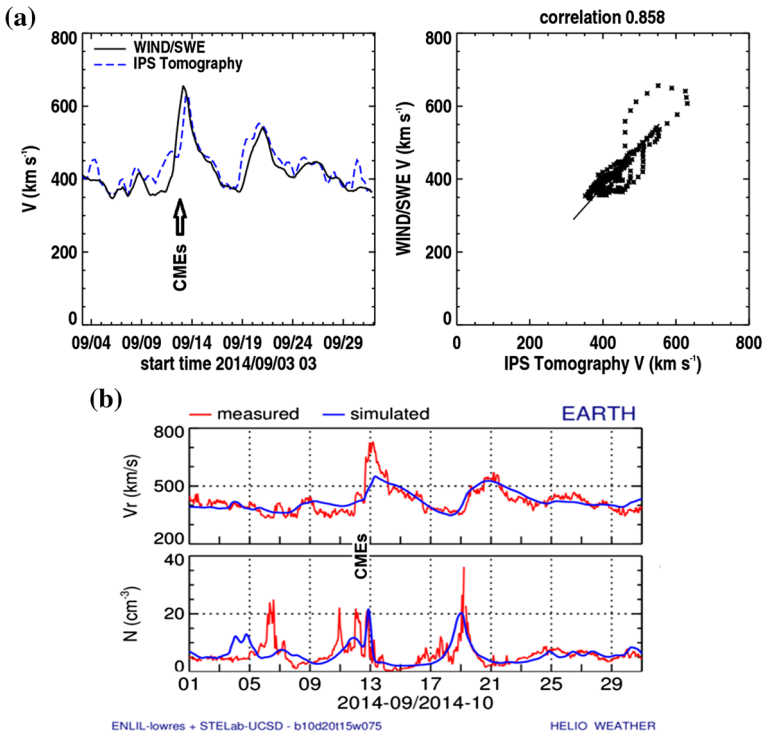
Fig. 9 a *Top left* Heliospheric density values (*dashed line*) at Earth determined from a tomographic analysis made using STELab. Japan IPS data recorded over a month of data in September 2014 compared with in situ measurements obtained at the Wind spacecraft. The times of the CMEs initiated on 9–10 September are indicated by the *arrow*. *Top right* Correlation between measured and predicted data. **b** (*Bottom*); heliospheric speed and density values from IPS driven ENLIL modelling at Earth compared with OMNI, hour-averaged, in situ measurements made over approximately the same time interval. The CME times in the OMNI data are indicated on the *plot*
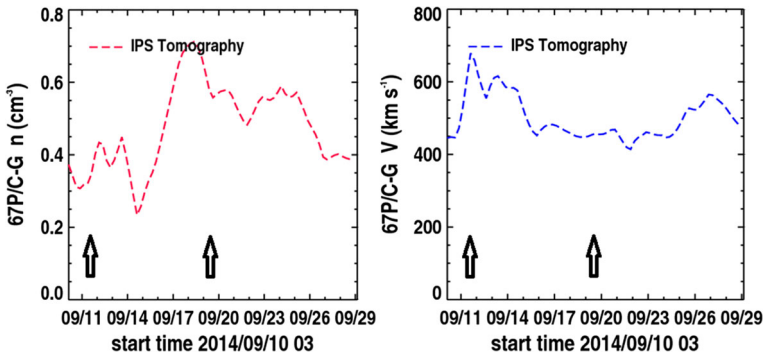

Fig. 10 The density (*left*) and speed (*right*) at Rosetta derived from kinematic 3D-reconstructions for the period 10–29 September 2014. The times of the two events as seen at Rosetta are indicated on both plots by *arrows*
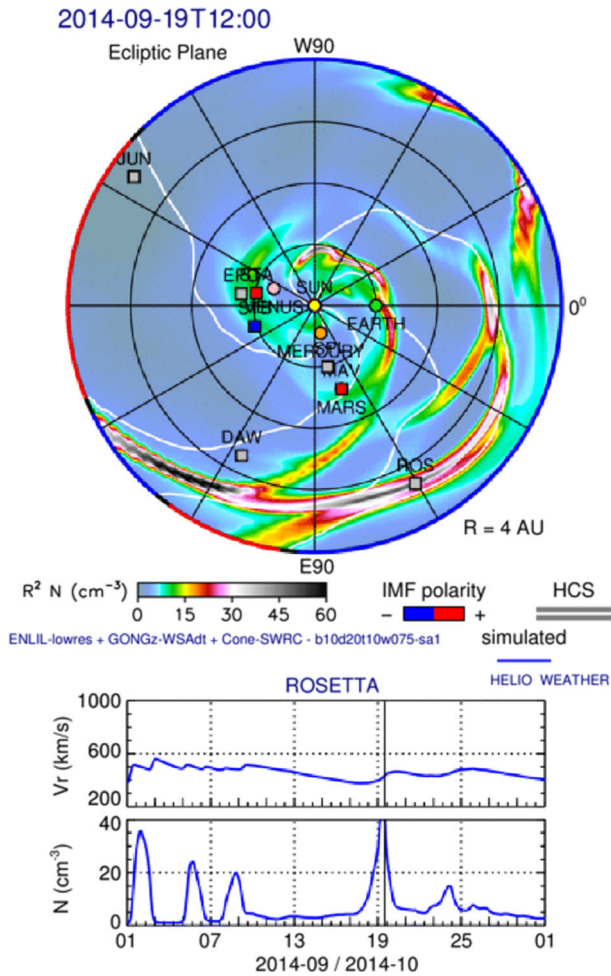
Fig. 11 *Top* An IPS driven ENLIL model ecliptic plot showing density enhancements from shocks and outward flowing CME material at 12:00 UT on 19 September 2014. The heliospheric current sheet/HCS sector boundaries in interplanetary space projected onto the ecliptic are indicated by a *white line* (represented on the icon between parallel *bars*). *Bottom* Heliospheric speed and density values at Rosetta derived from IPS driven ENLIL modeling. The time of the 19 September event observed at Rosetta is indicated by the *vertical solid timeline*

7 Measurements made by MAG and IES Aboard Rosetta in September 2014

Some of, but not all that is visible in the MAG data is due to the interaction of the solar wind with the (lightly outgassing) cometary obstacle. In this regard, waves with frequencies of about 20–50 mHz (Richter et al. 2015) were recorded at Rosetta from August 2014 and continue up to the present time (May, 2015). A general increase in the amplitudes of the waves was observed to be associated with increasing cometary activity. In addition

the wave intensity, which showed a dependence on the increasing solar-comet distance, was modulated by the occurrences (see below) of solar related density variations.

7.1 Magnetic and IES Data Recorded on 11 September and 19 September 2014 Aboard Rosetta

Figure 12 displays the magnetic field components measured by the outboard sensor of the magnetometer MAG aboard Rosetta on 11 September 2014. These components are displayed in *Comet-centered Solar EQuatorial* (CSEQ) coordinates, where +X (green) points from the comet to the Sun, the +z (BLUE) axis is the component of the Sun's north-pole (on the given date) orthogonal to the +X axis, and the +Y (red) axis completes the right-handed frame. On 11 September the position of Rosetta was about 30 km away from the comet.

Figure 12 shows that, on 11 September at ∼16:15 UT, there was a jump of about (−8, −9, +10) nT in the magnetic field data. It is noted that, at the same time there was a jump in the ion energy and increased ion count rates were measured by the IES instrument (see Fig. 13). After this jump the magnetic field stayed relatively calm for some hours. Thereafter, an increased level of turbulence—after a sharp jump in the By component of
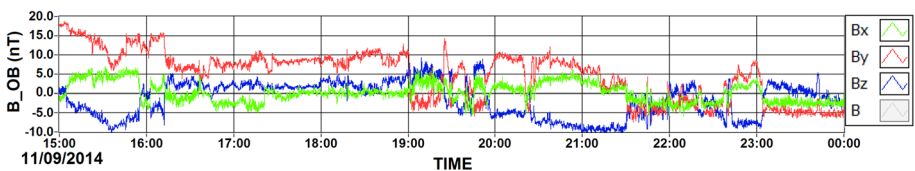

Fig. 12 The magnetic field components recorded by MAG on 11 September 2014 from 15:00 to 24:00 UT, where +X (*green*) points from the comet to the Sun, the +z (*blue*) axis is the component of the Sun's north-pole (on that date) orthogonal to the +X axis, and the +Y (*red*) axis completes the right-handed frame. The data are plotted in CSEQ coordinates and they are 10 mHz low-pass filtered
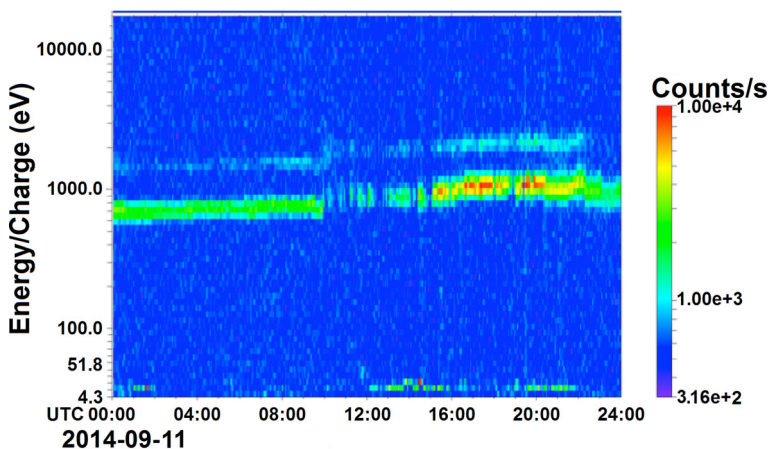

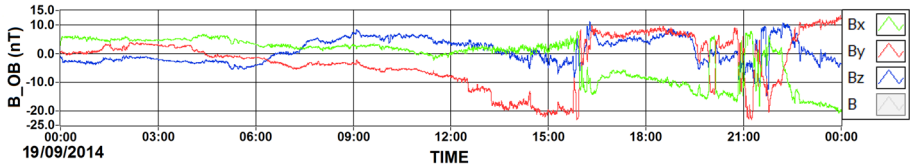**Fig. 13** Count rates measured by the IES on 11 September 2014

Fig. 14 The magnetic field components recorded by MAG on 19 September 2014 using the same conventions adopted in Fig. 12
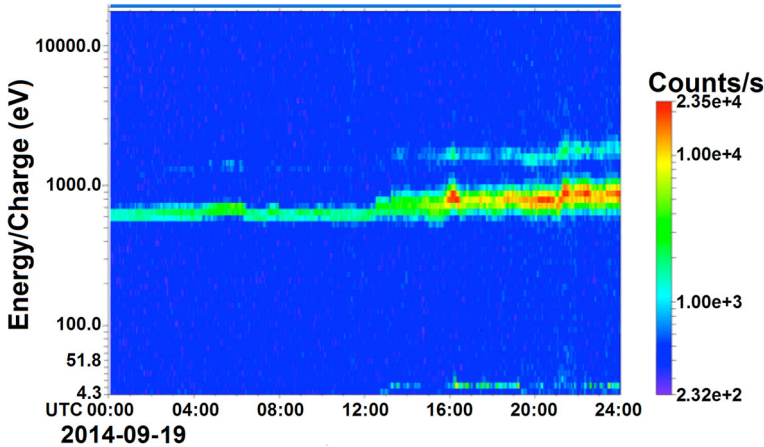

Fig. 15 Ion count rates recorded by the IES on 19 September 2014

-13 nT between $\sim$1930 UT and 20:00 UT—was recorded. In this time interval the ion count rate measured by the IES was very high (Fig. 13).

Figure 14 presents the magnetic field components measured by MAG on 19 September in CSEQ coordinates using the same conventions adopted in Fig. 12. These data show that, on 19 September at $\sim$15:55 UT the magnetic field jumped by about $(-20, +30, 0)$ nT. Before that time, conditions were very smooth and stable. Some 3 h later, after 20:00 U.T., a highly variable field with large scale fluctuations of up to $\sim$30 nT was present. These turbulent signatures lasted until 23 September 2014.

The beginning of the perturbed interval was characterized in IES data by high ion counts (Fig. 15). Especially between 20:00 and 22:30 UT the huge, and very rapid, magnetic field oscillations recorded by MAG coincided with the maximum enhanced ion count rates measured by the IES.

8 General Discussion

8.1 SREM Results

The element abundances characterizing impulsive SEPs, as described by Cane et al. (1986) and Reames (1999, 2013), result from resonant stochastic acceleration in magnetic reconnection regions that incorporate open magnetic field lines, allowing both accelerated

ions and ejected plasma to escape from a flare site. Impulsive SEPs are generally limited to within a 30° longitude band about the foot-point of the nominal field line magnetically connected to their parent active region.

The magnetic connection from Rosetta to the Sun was generally 180° or greater away from Rosetta during September 2014 and, thus, the spacecraft was more directly connected to the rear-side of the Sun than was Earth. In the case of the flare on 1 September 2014 it should be noted that energetic particles were observed at Earth and at Rosetta, as well as by the STEREO energetic particle sensors—when STEREO was located far behind the Sun as seen from Earth. Figure 16 shows signatures of this prompt event from the rear side of the Sun at the comet, which was recorded about 30 min after flare initiation and endured until ∼9 September 2014 in each of the three different energy channels of SREM/Rosetta which are sensitive to protons with energies >12, >27 and >49 MeV respectively. This figure provides (relative to Fig. 4) an indication of the energy spectrum of the event.

No perceptible SEP was observed in SREM data in association with the major flare of 10 September 2014. This was probably due to the fact (see Fig. 2) that MeV particles comprised a minor part of the accelerated population. Also, the induced magnetic field building up at the comet at that time (Nilsson et al. 2015) could have shielded the nucleus from the arrival of particles of moderate energies (see Kallio et al. 2012 for an account of particle shielding by the induced magnetic field at Mars).

It is noted that impulsive events were observed reasonably frequently at Rosetta in SREM data during the inbound leg of its trajectory around the Sun.
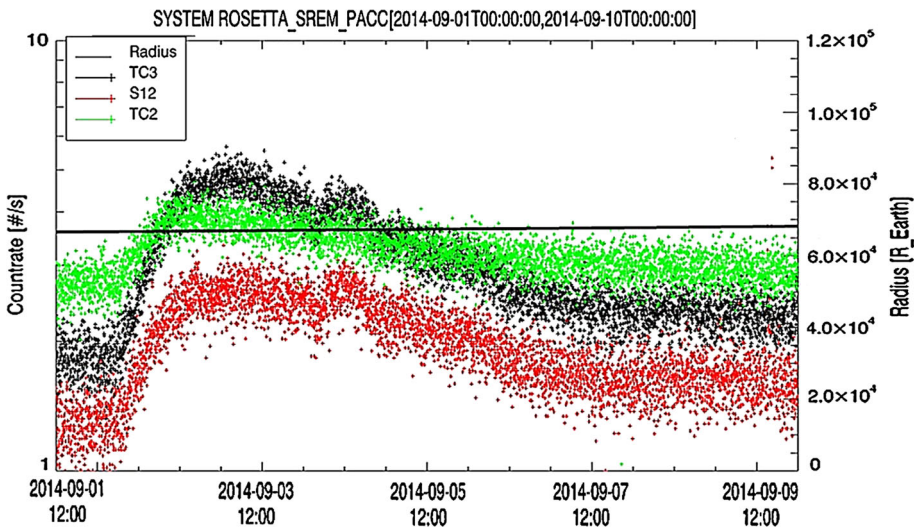

Fig. 16 Signatures of a prompt energetic particle event from the rear side of the Sun recorded between 01 and ∼09 September 2014 in three different energy channels of SREM/Rosetta which are sensitive to protons with energies >12 MeV (TC3), >27 MeV (S12) and >49 MeV (TC2) respectively. Also shown is the distance at the time of the measurements between the Rosetta spacecraft and the Earth in units of Earth radii

8.2 MAG Results

The magnetometer on-board Rosetta (RPC-MAG) has the capability to measure all three components of the magnetic field in the close vicinity of comet 67P/Churyumov–Gerasimenko. From August 2014 the measured magnetic field has been observed to become progressively more influenced by the comet as the solar wind continues to interact with this, gradually waxing, outgassing object. During this time, as already mentioned above, an induced magnetosphere has been building up (Nilsson et al. 2015). The comet itself has no intrinsic magnetic field (Auster et al. 2015).

As described in Sect. 4, solar ejecta that exited the Sun on 1 September and 9–10 September 2014 were each predicted to reach the position of ROSETTA after about 10 days. Striking magnetic signatures were registered at $\sim$15:55 UT on 11 September and at 19:00 UT on 19 September 2014. Both of these events were characterized by a significant polarity change in the By field component, succeeded by huge wave activity during the following $\sim$30 min.

The topological behaviour of the above mentioned events was different. On 11 September the field was relatively featureless at first and then it jumped. On 19 September the Bx component increased steadily over several hours before making a jump. Meanwhile, the By component decreased in parallel, also over hours, starting at about 12:30 UT (although during this decrease it executed a few minor jumps). The significant jump recorded at $\sim$16:00 tracks both components back to values which could be expected to be present without any ensuing particle event.

An in depth minimum variance analysis reveals that the shock on 19 September involved a reversal of only one component. This means that the magnetic field vector rotated by about 90° in the xz-plane of the Minimum Variance System. The normal to this discontinuity pointed directly in the Min.Var. direction, which can be expressed as (0.85, 0.45, −0.28) in CSEQ coordinates, see Fig. 17. The shock normal assumed an angle of about 31° to the comet–Sun line.

8.3 IES Results

The IES measurements illustrated in Figs. 13 and 15 show solar wind proton and alpha particle measurements at energies greater than 500 eV. Increases in solar wind proton and alpha particle energies due to the arrivals of predicted CME events at the spacecraft can clearly be seen in the data. In addition to the solar wind measurements, new-born cometary pickup ions (Nilsson et al. 2015) are identified to be present in the lowest energy channels. The energies of these newly produced ions are less than 1 eV but they appear to have a higher energy in the IES measurements due to negative spacecraft charging. When a
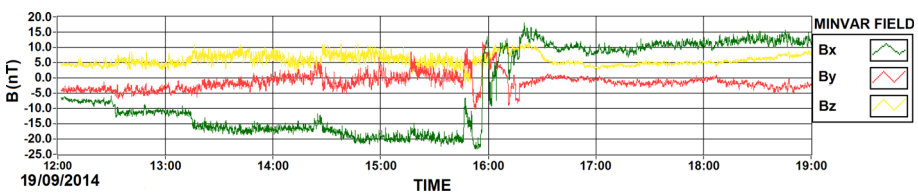

Fig. 17 The magnetic field rotated to a Minimum Variance System (maximum variance component: *green*; minimum variance direction: *yellow*)

spacecraft charges to negative values, low energy ions in the ambient environment are accelerated into on-board particle instruments and appear at energies equal to their ambient energy plus the spacecraft potential (Mandt et al. 2012). On both dates (11 September and 19 September) the low energy ion signal became stronger and was seen to display higher energies after CMEs passed the spacecraft, thereby showing the clear influence exerted by CMEs on the spacecraft environment.

8.4 Shock Associated CMEs at Rosetta

Gradual SEP Events are characterized inter alia by their: relatively long durations (days), wide spread in longitude (up to $\sim 180°$ in extreme cases) and association with fast CME driven shocks. In the latter context, as a CME propagates into the interplanetary environment it carries with it, frozen into the ejected mass, the local solar surface magnetic field. In a transition region between the normal sectored magnetic field structure of interplanetary space and the fields frozen into the ejected material, a shock is formed (Wilson et al. 2004) within which constituents of the interplanetary plasma are accelerated to form a solar particle event.

In the case of a fast CME, particle acceleration begins as the shock forms in the solar corona and continues as it advances outward, while accelerating particles that flow forward over an extremely wide front that can cover up to half of the inner heliosphere. As described by Reames (2013), "shock acceleration takes place as ions are scattered back and forth across the shock by resonant Alfvén waves, amplified by the accelerated protons themselves as they stream away". The most efficient acceleration takes place near the 'nose' of the shock ahead of the CME and, in consequence, the intensity-time profiles of gradual SEP events (electrons and ions) show significant variability from one event to another (Lario and Simnett 2004; Vainio et al. 2009; Watermann et al. 2009). Signatures due to the arrival at the comet of shock related CMEs identified in MAG and IES data are interpreted to be due to the propagation of CME driven shocks to Rosetta that exited the Sun on 1, 9 and 10 September 2014. No energetic particle event was recorded by SREM at these arrival times.

8.5 Sputtering at the Comet

The ROSINA experiment on Rosetta detected metal atoms which are interpreted to be associated with refractory materials and not volatile ice (Haessig et al. 2015; Le Roy et al. 2015). From studies of the exospheres of the Moon and Mercury, it is known that several mechanisms could be effective in ejecting Na, K, and Si atoms from the nucleus surface of comet 67P (Killeen and Ip 1999). These include photon-stimulated desorption (McGrath et al. 1986), impact vaporization (Cremonese et al. 2005), and ion sputtering (Potter and Morgan 1988a, b). In the present context the third effect (i.e., surface sputtering by solar wind ions) is of particular interest even though the other effects would contribute. Wurz et al. (2015) reported that the relative abundances of Na, K and Si measured by ROSINA/ Rosetta at a heliocentric distance of about 3.0–3.5 AU exhibited anti-correlation with the total gas production rates of H_2O, CO and CO_2 measured by the Comet Pressure Sensor. The explanation is simply that when the gas production rate (near the "neck" region) was high, the column number density of the neutral coma molecules was just large enough to shield the surface of the nucleus from the solar wind flux but when the gas production rate (near the "head" and the "body" region) was a factor of 2–3 lower, the solar wind could impinge on the nuclear surface and sputter refractory grains effectively, leading to the

emission of heavy metal atoms. One can therefore arrive at an interesting conclusion that, unlike the cases of the Moon and Mercury, photon-stimulated desorption and impact vaporization are not important in the sputtering process, at least, at the above-mentioned heliocentric range.

Killeen et al. (2012) studied the sputtering effect on the lunar exosphere by the passage of a CME and found that the sputtering production rates between the quiet solar wind condition and a CME of nominal size could amount to a factor of 50 on taking into account the He^{2+} and heavy ions like O^{7+} which are enhanced in CMEs. This means that, if the CME events of 1 September and 9–10 September hit comet 67P during a period of low outgassing, an enhanced flux of Na, K and Si atoms relative to quiet solar wind conditions should be detected by ROSINA.

Wurz et al. (2015) remarked that once the gas production rate of comet 67P near perihelion is large enough and the whole surface of the cometary nucleus is shielded from solar wind flux, the corresponding effect will diminish. This might be the case, but the enhanced solar wind flux of a CME can interact with the dust grains present in the extended coma which have been found to be enriched in Na (Schulz et al. 2015). Furthermore, the SEPs associated with CME driven shocks could produce an additional sputtering effect.

9 Conclusions

- Solar activity on 1 September and 9–10 September 2014 produced responses at comet 67P/C–G when it was located at ~ 3.7 AU.
- A flare on 1 September 2014 produced an MeV particle event in SREM data which began ~ 30 min after flare initiation and is interpreted to have constituted an Impulsive SEP.
- IPS modelling can provide low-resolution velocity and density forecasts of the arrival at various heliospheric locations of time-variable heliospheric structures (CME driven shocks) propagating away from the Sun to a distance of at least 4 AU.
- The ENLIL model driven by IPS as well as operated using cone model and WSA inputs can also track outward travelling CME driven shocks over approximately 10 days.
- The predictions of these models of the arrival at Rosetta/Comet 67P/C–G of three CME related disturbances corresponded satisfactorily with strong signatures observed in MAG and IES data, thereby providing confidence that the signatures recorded aboard the spacecraft were solar related and traceable to particular events.
- Photon-stimulated desorption and impact vaporization are deduced not to have been important in the sputtering process at the comet when it was located at ~ 3.5 AU. At locations closer to perihelion, despite enhanced shielding of the nucleus from solar wind flux, energetic particles associated with significant solar activity can be expected to stimulate sputtering.

References

C.N. Arge, V.J. Pizzo, Improvement in the prediction of solar wind conditions using near real time solar magnetic field updates. J. Geophys. Res. **105**, 10465–10480 (2000)

H.-U. Auster, I. Apathy, G. Berghofer, K.-H. Fornacan, A. Remizov, C. Carr, C. Güttler, G. Haerendel, P. Heinisch, D. Hercik, M. Hilchenbach, E. Kührt, W. Magnes, U. Motschmann, I. Richter, C.T. Russell,

A. Przyklenk, K. Schwingenschuh, H. Sierks, K.-H. Glassmeier, The nonmagnetic nucleus of comet 67P/Churyumov–Gerasimenko. Science (2015). doi:10.1126/science.aaa5102

J.L. Burch, R. Goldstein, T.E. Cravens, W.C. Gibson, R.N. Lundin, C.J. Pollock, J.D. Winningham, D.T. Young, RPC-IES: the ion and electron sensor of the Rosetta Plasma Consortium. Space Sci. Rev. **28**(1–4), 697–712 (2007)

L.F. Burlaga, E. Sittler, F. Mariani, R. Schwenn, Magnetic loop behind an interplanetary shock: Voyager, Helios and IMP 8 observations. J. Geophys. Res. **86**, 6673–6684 (1981)

H.V. Cane, R.E. McGuire, T.T. von Rosenvinge, Two classes of solar energetic particle events associated with impulsive and long-duration soft X-ray flares. Astrophys. J. **301**, 448–459 (1986)

C. Carr, E. Cupido, C.G.Y. Lee, A. Balogh, T. Beek, J.L. Burch, C.N. Dunford, A.I. Eriksson, R. Gill, K.-H. Glassmeier, R. Goldstein, D. Lagoutte, R. Lundin, K. Lundin, B. Lybekk, J.L. Micheau, G. Musmann, H. Nilsson, C. Pollock, I. Richter, J.G. Trotignon, RPC: the Rosetta Plasma Consortium. Space Sci. Rev. **128**(1–4), 629–647 (2007)

G. Cremonese, M. Bruno, S. Marchi, Neutral sodium atoms release from the surfaces of the Moon and Mercury induced by meteoroid impacts. Mem. Soc. Astron. Ital. Suppl. **6**, 63–66 (2005)

M. Dryer (ed.), The August 1972 events (special issue). Space Sci. Rev. **19**, 4–5 (1976)

K.-H. Glassmeier, H. Boehnhardt, D. Koschny, E. Kührt, I. Richter, The Rosetta mission: flying towards the origin of the solar system. Space Sci. Rev. **128**(1–4), 1–21 (2007a)

K.-H. Glassmeier, I. Richter, A. Diedrich, G. Musmann, U. Auster, U. Motschmann, A. Balogh, C. Carr, E. Cupido, A. Coates, M. Rother, K. Schwingenschuh, K. Szegö, B. Tsurutani, The fluxgate magnetometer in the Rosetta Plasma Consortium. Space Sci. Rev. **128**, 649–670 (2007b)

N. Gopalswamy, A. Lara, R.P. Lepping, M.L. Kaiser, D. Berdichevsky, O.C. St. Cyr, Interplanetary acceleration of coronal mass ejections. Geophys. Res. Lett. **27**(2), 145–148 (2000)

M. Haessig, K. Altwegg, H. Balsiger, A. Bar-Nun, J.J. Berthelier, A. Bieler, P. Bochsler, C. Briois, U. Calmonte, M. Combi, J. De Keyser, P. Eberhardt, B. Fiethe, S.A. Fuselier, M. Galand, S. Gasc, T.I. Gombosi, K.C. Hansen, A. Jäckel, H.U. Keller, E. Kopp, A. Korth, E. Kührt, L. Le Roy, U. Mall, B. Marty, O. Mousis, T. Owen, H. Rème, M. Rubin, T. Sémon, C. Tornow, C.-Y. Tzou, J.H. Waite, P. Wurz, Time variability and heterogeneity in the coma of 67P/Churyumov–Gerasimenko. Science (2015). doi:10.1126/science.aaa0276

R.A. Howard, J.D. Moses, A. Vourlidas, J.S. Newmark, D.G. Socker, S.P. Plunkett, C.M. Korendyke, J.W. Cook, A. Hurley, J.M. Davila, W.T. Thompson, O.C. St, E. Cyr, K. Mentzell, J.R. Mehalick, J.P. Lemen, D.W. Wuelser, T.D. Duncan, C.J. Tarbell, A.Moore Wolfson, R.A. Harrison, N.R. Waltham, J. Lang, C.J. Davis, C.J. Eyles, H. Mapson-Menard, G.M. Simnett, J.P. Halain, J.M. Defise, E. Mazy, P. Rochus, R. Mercier, M.F. Ravet, F. Delmotte, F. Auchere, J.P. Delaboudiniere, V. Bothmer, W. Deutsch, D. Wang, N. Rich, S. Cooper, V. Stephens, G. Maahs, R. Baugh, D. McMullin, T. Carter, Sun Earth connection coronal and heliospheric investigation (SECCHI). Space Sci. Rev. **136**, 67 (2008). doi:10.1007/s11214-008-9341-4

B.V. Jackson, P.L. Hick, M. Kojima, A. Yokobe, Heliospheric tomography using interplanetary scintillation observations 1. Combined Nagoya and Cambridge data. J. Geophys. Res. **103**, 12049–12068 (1998)

B.V. Jackson, A. Buffington, P.P. Hick, R.C. Altrock, S. Figueroa, P.E. Holladay, J.C. Johnston, S.W. Kahler, J.B. Mozer, S. Price, R.R. Radick, R. Sagalyn, D. Sinclair, G.M. Simnett, C.J. Eyles, M.P. Cooke, S.J. Tappin, T. Kuchar, D. Mizuno, D.F. Webb, P.A. Anderson, S.L. Keil, R.E. Gold, N.R. Waltham, The solar mass ejection imager (SMEI) mission. Sol. Phys. **225**, 177–207 (2004)

B.V. Jackson, P.P. Hick, Three-dimensional tomography of interplanetary disturbances, in *Chapter 17 in Solar and Space Weather Radiophysics, Current Status and Future Developments. Astrophysics Space Science Library*, vol. 314, ed. by D.E. Gary, C.U. Keller (Kluwer Academic Publisher, Dordrecht, 2005), pp. 355–386

B.V. Jackson, A. Buffington, P.P. Hick, X. Wang, D. Webb, Preliminary three-dimensional analysis of the heliospheric response to the 28 October 2003 CME using SMEI white-light observations. J. Geophys. Res. **111**(A4), A404S91 (2006)

B.V. Jackson, The 3D analysis of the heliosphere using interplanetary scintillation and Thomson-scattering observations. Adv. Geosci. **30**, 69–91 (2011)

B.V. Jackson, D. Odstrčil, H.-S. Yu, P.P. Hick, A. Buffington, J.C. Mejia-Ambriz, J. Kim, S. Hong, Y. Kim, J. Han, M. Tokumaru, The UCSD kinematic IPS solar wind boundary and its use in the ENLIL 3-D MHD prediction model. Space Weather **13**, 104–115 (2015). doi:10.1002/2014SW001130

M.L. Kaiser, T.A. Kucera, J.M. Davila, O.C. St Cyr, M. Guhathakurta, E. Christian, The STEREO mission: an introduction. Space Sci. Rev. **136**(1–4), 5–16 (2008)

E. Kallio, S. McKenna-Lawlor, M. Alho, R. Jarvinen, S. Dyadechkin, V.V. Afonin, Energetic protons at Mars: interpretation of SLED/Phobos-2 observations by a kinetic model. Ann. Geophys. **30**, 1595–1609 (2012)

R.M. Killeen, W.-H. Ip, The surface-bounded atmospheres of Mercury and the Moon. Rev. Geophys. **37**(3), 361–406 (1999). doi:10.1029/1999RG900001

R.M. Killeen, D.M. Hurley, W.M. Farrell, The effect on the lunar exosphere of a coronal mass ejection passage. J. Geophys. Res. (2012). doi:10.1029/2011JE004011

D. Lario, G.M. Simnett, Solar energetic particle variations, in "Solar variability and its effects on climate". Geophys. Mon. Ser. (AGU) **141**, 195–216 (2004)

L. Le Roy, K. Altwegg, H. Balsiger, J.J. Berthelier, A. Bieler, C. Briois, U. Calmonte, M.R. Combi, J. De Keyser, F. Dhooghe, B. Fiethe, S.A. Fuselier, S. Gasc, T.I. Gombosi, M. Hässig, A. Jäckel, M. Rubin, C.Y. Tzou, Inventory of the volatiles on comet 67P/Churyumov-Gerasimenko from Rosetta/ROSINA. Astron. Astrophys. **503** (2015). doi:10.1051/0004-6361/201526450

K.E. Mandt, D.A. Gell, M. Perry, J.H. Waite Jr, F.A. Crary, D. Young, B.A. Magee, J.H. Westlake, T. Cravens, W. Kasprzak, G. Miller, J.-E. Wahlund, K. Ågren, N.J.T. Edberg, A.N. Heays, B.R. Lewis, S.T. Gibson, V. de la Haye, M.-C. Liang, Ion densities and composition of Titan's upper atmosphere derived from the Cassini ion neutral mass spectrometer: analysis methods and comparison of measured ion densities to photochemical model simulations. J. Geophys. Res. **117**, E10006 (2012)

H. Mavromichalaki, A. Papaioannon, M. Gerontidon, I. Daglis, A. Anastasiadis, I. Sandberg, K. Tziotzion, I. Panagopoulos, P. Nieminen, A. Glover, P. Bühler, Solar particle event analysis using the ESA Standard Radiation Environment Monitor and the Worldwide Neutron Monitor network. In Proceedings 31st international cosmic ray conference Lodz (2009), pp. 1–4

M.A. McGrath, R.E. Johnson, L.T. Lanzerotti, Sputtering of sodium on the planet Mercury. Nature **323**, 694–696 (1986)

A. Mohammadzadeh, H. Evans, P. Nieminen, E. Daly, P. Vuilleumier, P. Bühler, C. Eggel, W. Hajdas, N. Schlumpf, A. Zehnder, J. Schmeider, R. Fear, The ESA Standard Radiation Environment Monitor Program: first results from PROBA-1 and INTEGRAL. IEEE Trans. Nucl. Sci. **50**(6), 2272–2277 (2003)

H. Nilsson, G.S. Wieser, E. Behar, C.S. Wedlund, H. Gunell, M. Yamauchi, R. Lundin, S. Barabash, M. Wieser, C. Carr, E. Cupido, J.L. Burch, A. Fedorov, J.-A. Sauvaud, H. Koskinen, E. Kallio, J.-P. Lebreton, A. Eriksson, N. Edberg, R. Goldstein, P. Henri, C. Koenders, P. Mokashi, Z. Nemeth, I. Richter, K. Szego, M. Volwerk, C. Vallat, M. Rubin, Birth of a comet magnetosphere: a spring of water. Science **347**(6220), aaa0571 (2015). doi:10.1126/science.aaa0571

D. Odstrčil, Modelling 3-D solar wind structure. Adv. Space Res. **32**, 497–506 (2003)

D. Odstrčil, V.J. Pizzo, Three-dimensional propagation of CMEs in a structured solar wind flow: 1. CME launched within the streamer belt. J. Geophys. Res. **104**, 483–492 (1999a). doi:10.1029/1998JA900019

D. Odstrčil, V.J. Pizzo, Three-dimensional propagation of coronal mass ejections in a structured solar wind flow 2. CME launched adjacent to the streamer belt. J. Geophys. Res. **104**, 493–504 (1999b). doi:10.1029/1998JA900038

K.W. Ogilvie, G.K. Parks, First results from WIND spacecraft: an introduction. Geophys. Res. Lett. **23**(10), 1179–1181 (1996)

O. Pace, D. Pawlak, C. Winkler, Integral mission and satellite. Astrophys. J. Suppl. Ser. **92**, 339–342 (1994)

A.E. Potter Jr, T.H. Morgan, Discovery of sodium and potassium vapour in the atmosphere of the Moon. Science **241**, 675–679 (1988a)

A.E. Potter Jr, T.H. Morgan, Extended sodium atmosphere of the Moon. Geophys. Res. Lett. **15**, 1515–1518 (1988b)

D.V. Reames, Particle acceleration at the Sun and in the heliosphere. Space Sci. Rev. **90**, 413–491 (1999)

D.V. Reames, The two sources of solar energetic particles. Space Sci. Rev. **175**, 53–92 (2013)

I. Richter, C. Koenders, H.-U. Auster, D. Fruehauff, C. Goetz, P. Heinisch, C. Perschke, U. Motschmann, B. Stoll, K. Altwegg, J. Burch, C. Carr, E. Cupido, A. Eriksson, P. Henri, R. Goldstein, J.-P. Lebreton, P. Mokashi, Z. Nemeth, H. Nilsson, M. Rubin, K. Szegoe, B.T. Tsurutani, C. Vallat, M. Volwerk, K.-H. Glassmeier, Observation of a new type of low frequency waves at comet 67P/Churyumov-Gerasimenko. Ann. Geophys. **8**(33), 1031–1036 (2015)

I. Sandberg, I.A. Daglis, A. Anastasiadis, P. Bühler, P. Nieminen, H. Evans, Unfolding and validation of SREM fluxes. IEEE Trans. Nucl. Sci. **59**(4), 1105–1112 (2012)

R. Schulz, M. Hilchenbach, Y. Langevin, J. Kissel, J. Silen, C. Briois, C. Engrand, K. Hornung, D. Baklouti, A. Bardyn, H. Cottin, H. Fischer, N. Fray, M. Godard, H. Lehto, L. Le Roy, S. Merouane, F.-R. Orthous-Daunay, J. Paquette, J. Rynö, S. Siljeström, O. Stenzel, L. Thirkell, K. Varmuza, B. Zaprudin, Comet 67P/Churyumov–Gerasimenko sheds dust coat accumulated over the past four years. Nat. Lett. **518**(7538), 216–218 (2015)

A. Taktakishvili, M. Kuznetsova, P. MacNeice, M. Hesse, I. Rastaetter, A. Pulkkinenen, A. Chulaki, D. Odstrčil, Validation of the coronal mass ejection predictions at the Earth orbit estimated by ENLIL heliospheric cone model. Space Weather (2009). doi:10.1029/2008SW000448

H.-S. Yu, B.V. Jackson, P.P. Hick, A. Buffington, D. Odstrčil, C.-C. Wu, J.A. Davies, M.M. Bisi, M. Tokumaru, 3D reconstruction of interplanetary scintillation (IPS) remote-sensing data: global solar wind boundaries for driving 3D-MHD models. Sol. Phys. (2015). doi:10.1007/s11207-015-0685-0

R. Vainio, L. Desorgher, E. Flückinger, M. Storini, R.B. Horne, G.A. Kovaltsov, K. Kudela, M. Laurenza, S. McKenna-Lawlor, H. Rothkaehl, I.G. Usoskin, Dynamics of the earth's particle radiation environment. Space Sci. Rev. **147**(3–4), 187–231 (2009)

J. Watermann, P. Wintoft, B. Sanahuja, E. Saiz, S. Poedts, M. Palmroth, A. Milillo, F.-A. Metallinou, C. Jacobs, N.Y. Ganushkina, I.A. Daglis, C. Cid, Y. Cerrato, G. Balasis, A.D. Aylward, A. Aran, Models of solar wind structures and their interaction with the Earth's space environment. Space Sci. Rev. **147**(3–4), 233–270 (2009)

J.W. Wilson, M.S. Clowdsley, F.A. Cucinotta, R.K. Tripathi, J.E. Nealy, G. DeAngelis, Deep space environments for human exploration. Adv. Space Res. **34**, 1281–1287 (2004)

P. Wurz, M. Rubin, K. Altwegg, H. Balsiger, S. Gasc, A. Galli, A. Jäckel, L. Le Roy, U. Calmonte, C.-Y. Tzou, U. Mall, A. Korth, B. Fiethe, J. De Keyser, J.-J. Berthelier, H. Rème, T. Gombosi, S. Fuselier, Solar wind sputtering from the surface of comet Churyumov-Gerasimenko. Astron. Astrophys. **583** (2015). doi:10.1051/0004-6361/201525980